ACS OMEGA

http://pubs.acs.org/journal/acsodf

Article

Selective Phonon Stimulation Mechanism to Tune Thermal Transport

Gaurav Kumar and Peter W. Chung*

Cite This: *ACS Omega* 2022, 7, 12787−12794

Read Online

ACCESS | Metrics & More | Article Recommendations | Supporting Information

ABSTRACT: In this paper, we determine the degree to which changes can be induced in the equilibrium thermal diffusivity and conductivity of a material via a selective nonequilibrium infrared stimulation mechanism for phonons. Using the molecular crystal RDX, we use detailed momentum-dependent coupling information across the entire Brillouin zone and the phonon gas model to show that stimulating selected modes in the spectrum of a target material can induce substantial changes in the overall thermal transport properties. Specifically in the case of RDX, stimulating modes at ∼22.74 cm^{-1} over a linewidth of 1 cm^{-1} can lead to enhanced scattering rates that reduce the overall thermal diffusivity and conductivity by 15.58 and 12.46%, respectively, from their equilibrium values. Due to the rich spectral content in the materials, however, stimulating modes near ∼1140.67 cm^{-1} over a similar bandwidth can produce an increase in the thermal diffusivity and conductivity by 55.73 and 144.07%, respectively. The large changes suggest a mechanism to evoke substantially modulated thermal transport properties through light−matter interaction.

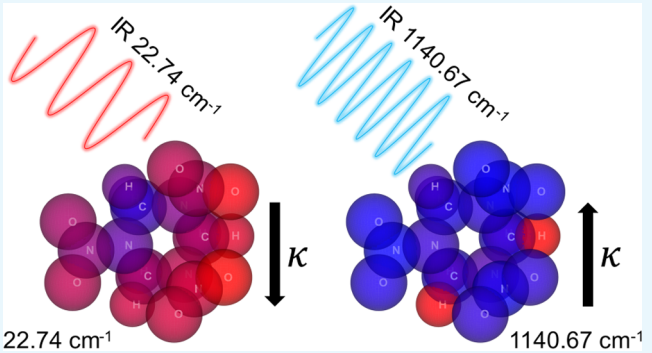

INTRODUCTION

The use of strong optical pulses in far-to-mid infrared (IR) range (0.1−100 THz) with optical power ranging from milli-Watts to several Watts has emerged as a powerful tool to study material properties in solid-state and condensed matter systems under nonequilibrium conditions.[1−15] In particular, in energetic materials where phonons are the primary carriers of heat, ultrafast laser heating and spectroscopy have enabled the investigation of shock-induced chemistry[16−18] and subpicosecond vibrational energy-transfer dynamics[19−22] to form a more complete understanding of the shock-to-initiation process.

For a molecular crystal to absorb IR radiation, the light must interact with the electrons to induce molecular dipoles at frequencies that match phonon mode frequencies ($\omega_{IR} = \omega_{ph}$). At equilibrium, phonon populations follow Bose−Einstein statistics.[23] However, the absorption of optical energy leads to a nonequilibrium distribution of phonons (and/or electrons), which, in turn, will lead to significant changes in phonon−phonon (and/or electron−phonon) scattering rates and evoke a nonequilibrium thermal transport mechanism.[24−30] Efforts have traditionally used structurally induced changes to the intrinsic scattering properties to affect thermal transport.[31] But new directions have investigated nondiffusive thermal transport by phonons upon optical excitation in which the phonon distribution has departed from equilibrium due to photoexcitation of the lattice.[25−28,32−34]

The inducement of nonequilibrium occurs in physical processes in many applications such as laser−matter interactions, irradiation in nuclear reactors, etc.[15,35] and is considered to be one of the reasons for a wide range of thermal conductivity values reported for single-layer graphene.[36−40] Selective stimulation mechanisms have been explored recently to tailor transient electron−phonon and phonon−phonon interactions over subpicosecond time through photoexcitations[41−47] as well as to understand the obfuscating role multiphonon scattering mechanisms play on single phonon dynamics.[42,48,49] The question then follows, "to what extent does selective stimulation affect the intrinsic lattice thermal conductivity and diffusivity of the target material?" It is not obvious a priori that selective stimulation will increase or decrease the overall transport properties of the material, if at all. This is partly because the relationship between atomic structure and thermal conductivity is highly nonlinear. According to Fermi's Golden Rule (FGR),[50] the transport properties depend on an integral over transition probabilities tied to the phonon dispersion (eigenvalues) and the

Received: December 29, 2021
Accepted: March 28, 2022
Published: April 7, 2022

anharmonic coupling between the modes that depend, in turn, on the chemical and physical structures of the material. However, this nonlinearity might be exploitable; stimulation of certain frequencies can possibly induce lower or higher thermal transport properties overall through a controlled disruption to the equilibrium scattering network. In the context of energetic materials, the lattice thermal properties are also strongly correlated to initiation properties;[51,52] insofar as phonons mediate thermal transport, controlling the degree to which phonons contribute to thermal transport may also afford control over thermally or vibrationally induced chemical reactions.

In this work, we perform a numerical experiment to explore how selective stimulation, by systematic perturbation of phonon occupation levels from equilibrium in narrow frequency bands in crystalline α-RDX, can modify the overall thermal transport properties of the material. We limit our consideration to three-phonon scattering processes under the single-mode relaxation time approximation (SMRTA)[53−55] and the contribution of propagating thermal carriers to thermal conductivity using the phonon gas model (PGM).[56−60]

RESULTS AND DISCUSSION

Figure 1 shows the average percent change in three-phonon scattering rates (% $\Delta\Gamma^{avg,\Phi_s}$) resulting from stimulating the 15

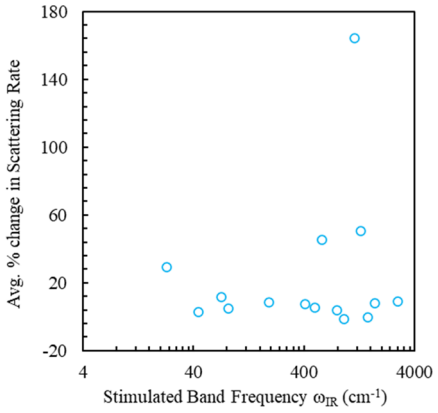

Figure 1. Average percent change in modewise scattering rates upon stimulating 15 frequency bands in RDX (stimulating one band at a time). Large increases in scattering rates are observed upon stimulating the bands at 22.74, 582.36, 1140.67, or 1299.72 cm^{-1}.

phonon bands one at a time. The definitions for measuring the effect of stimulation are provided in section S3 of the Supporting Information. The results indicate that a substantial increase in scattering rates can be achieved upon (a) stimulating the low-frequency band at 22.74 cm^{-1} resulting in an average ∼29% increase in the modewise scattering rates (average over 32,256 phonon modes in RDX) or (b) stimulating the mid-frequency band at 582.36, 1140.67, or 1299.72 cm^{-1} resulting in average ∼46, ∼165, or ∼51% increase in the modewise scattering rates, respectively. The low-frequency band at 22.74 cm^{-1} corresponds to molecular translation and the mid-frequency bands at 582.36, 1140.67, and 1299.72 cm^{-1} correspond to ring bending, twist, and rocking, CH_2 twist and rocking, and NN equatorial stretching and CH_2 rocking, respectively, as shown in Table S1 of the Supporting Information. The large change in scattering rates upon stimulating the low-frequency band can be attributed to a combination of two factors: (i) The lowest-frequency modes are responsible for over 99% of the mode-to-mode scattering (details can be found in our earlier work[61]) due to their strong anharmonic coupling with other modes and a large phase space volume available for three-phonon scattering and (ii) the majority of the low-frequency modes scatter via absorption processes ($\phi_1 + \phi_2 \rightarrow \phi_3$) involving two other low-frequency modes, and since the increase in the phonon population of the stimulated low-frequency modes is ∼120%, a proportionate ∼29% increase is observed in the scattering rates. This increase in scattering rates also leads to a substantial decrease in average modewise diffusivity and scalar thermal conductivity by 15.58 and 12.46%, respectively, as shown in Figures 2 and 3,

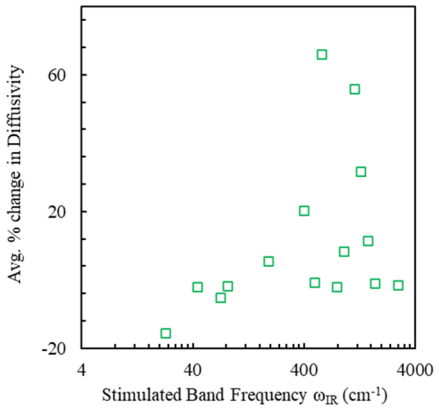

Figure 2. Average percent change in modewise diffusivities upon stimulating 15 frequency bands in RDX (stimulating one band at a time). A substantial decrease in the diffusivity is observed upon stimulating the low-frequency band at 22.74 cm^{-1}, and a substantial increase is observed upon stimulating the mid-frequency bands at 582.36, 1140.67, or 1299.72 cm^{-1}.

respectively. In contrast, the mid-frequency modes scatter primarily via emission processes ($\phi_1 \rightarrow \phi_2 + \phi_3$) involving another mid-frequency mode. Although these modes are less anharmonic compared to the lowest-frequency modes and therefore scatter less, the phonon population of the mid-frequency modes can increase by over 1000% resulting in an

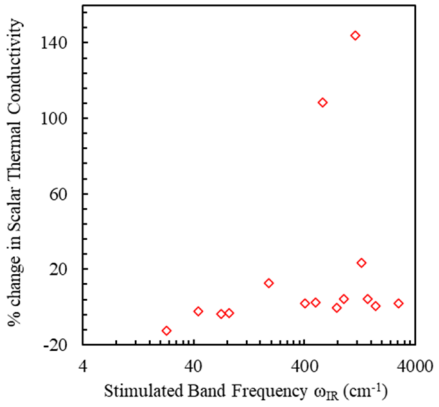

Figure 3. Percent change in the scalar thermal conductivity upon stimulating 15 frequency bands in RDX (stimulating one band at a time). A substantial decrease in the conductivity is observed upon stimulating the low-frequency band at 22.74 cm^{-1}, and a substantial increase is observed upon stimulating the mid-frequency bands at 582.36, 1140.67, or 1299.72 cm^{-1}.

https://doi.org/10.1021/acsomega.1c07364
ACS Omega 2022, 7, 12787−12794

overall large average percent increase in the scattering rates, as shown in Figure 1. It should also be noted that stimulating the band at 582.36, 1140.67, or 1299.72 cm^{-1} leads to a close to 100% decrease in the scattering rate for some of the mid-frequency modes. Specifically, stimulating the band at 1140.67 cm^{-1} leads to a ∼100% decrease in the scattering rate for a large number of modes at frequencies around 301, 550−580, 838, and 920 cm^{-1}, as shown in Figure 4, enabling those

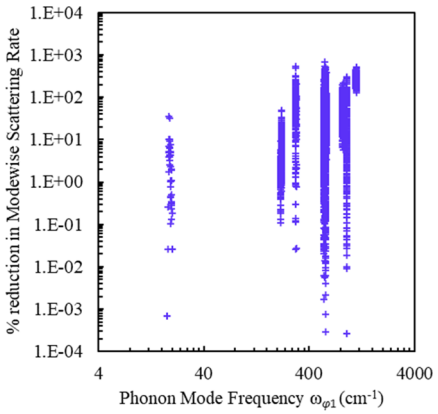

Figure 4. Percent reduction in modewise scattering rates upon stimulating the band at 1140.67 cm^{-1}. A close to 100% decrease in the scattering rate is observed for modes around 301, 550−580, 838, and 920 cm^{-1}. Negative values indicating an increase in the modewise scattering rate have been ignored due to the log scale.

modes to be frustrated to the point that they do not contribute to the scattering dynamics. Not surprisingly, such a large decrease means scattering rates are driven to near zero and the associated carriers now have very large mean free paths, as shown in Figure 5. As a result, stimulating the aforementioned mid-frequency bands leads to a substantial increase in the diffusivity and thermal conductivity in RDX, as shown in Figures 2 and 3, respectively. Since the thermal diffusivity represents the amount of heat that flows through the phonon modes (diffusivity is defined as the conductivity per unit specific heat), an increase in the diffusivity reduces the

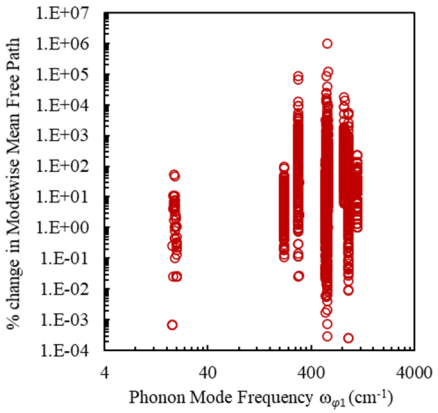

Figure 5. Percent change in modewise mean free paths upon stimulating the band at 1140.67 cm^{-1}. Due to an ∼100% decrease in scattering rates in some modes as shown in Figure 4, these modes have a very high mean free path leading to a large increase in the diffusivity and thermal conductivity, as shown in Figures 2 and 3, respectively. Negative values for % change in the modewise mean free path have been ignored due to the log scale.

possibility of localization of vibrational energy, which is important in the context of reaction initiation.[51,52,62] It should be expected that selectively stimulating the appropriate modes will increase or decrease reaction sensitivity. Table 1 identifies the top three-phonon bands in RDX whose selective stimulation will likely produce substantial increases/decreases in the thermal diffusivity and conductivity.

Table 1. Ranking of Phonon Bands in RDX Based on Their Ability to Increase or Decrease Thermal Diffusivity or Conductivity upon Stimulation[a]

ranking	1	2	3
increase diffusivity	582.36	1140.67	1299.72
decrease diffusivity	22.74	71.25	43.99
increase conductivity	1140.67	582.36	1299.72
decrease conductivity	22.74	71.25	83.38

[a]Numbers in the table represent the frequency of phonon bands in cm^{-1}.

Figure 6 (left) shows the modewise phonon lifetimes under equilibrium (before band stimulation) along with the largest and smallest modewise lifetime values after stimulating the 15 frequency bands. For each mode ϕ_1, the largest and smallest lifetimes after band stimulation are defined as $\tau^{\Phi_S}_{\phi_1,\max} = \max\{\tau^{\Phi_{S_i},\ i=1\text{ to }15}_{\phi_1}\}$ and $\tau^{\Phi_S}_{\phi_1,\min} = \min\{\tau^{\Phi_{S_i},\ i=1\text{ to }15}_{\phi_1}\}$, respectively. Figure 6 (right) shows the largest phonon lifetime across all 32,256 modes in RDX upon stimulating each frequency band, defined as $\tau^{\Phi_S}_{\phi,\max} = \max\{\tau^{\Phi_S}_{\phi_{i=1\text{ to }32,256}}\}$. Our results indicate that stimulating the modes can lead to an increase in modewise lifetime values up to four orders of magnitude. The largest % increase in lifetime is observed for several modes around ∼301, from ∼550 to ∼580 cm^{-1}, ∼838, and 920 cm^{-1}. The largest phonon lifetime across all 32,256 modes is observed to be 663.88 ps after stimulating the band at 582.36 cm^{-1}, 4784.26 ps after stimulating the band at 1299.72 cm^{-1}, and 2272.90 ps after stimulating all other bands. The largest phonon lifetime in the system indicates how long would the phonon distribution deviate from the equilibrium state caused by IR stimulation.

In our earlier work,[61] we showed that the phonon lifetimes estimated via FGR using three phonon scattering processes under SMRTA are in good agreement with the experimentally reported lifetime values.[63,64] The subpicosecond lifetimes for the low-frequency modes in RDX reported in our work are similar to the lifetimes reported by McGrane et al.[65] for other energetic materials like PETN, HMX, and TATB at 295 K. The relaxation times of the nitro group wagging and rotation modes and asymmetric stretching modes observed in our work are also similar to the values reported by Aubuchon et al.[66] and Ostrander et al.[67] Furthermore, the subpicosecond anisotropy decay due to scattering of the nitro group modes with the low-frequency phonon modes up to 192 cm^{-1} reported in our work is consistent with the observations made by Ramasesha et al. who used ultrafast infrared spectroscopy to probe a narrow band at 1533 cm^{-1} in thin-film RDX.[68] These suggest that the three phonon scattering model can provide an accurate description of the anharmonic coupling and the phonon−phonon relaxation process in RDX under ambient conditions.

The earlier calculations[69,70] based on PGM with three phonon scattering significantly underestimated the thermal conductivity; however, this is because PGM treats all phonons

https://doi.org/10.1021/acsomega.1c07364
ACS Omega 2022, 7, 12787−12794

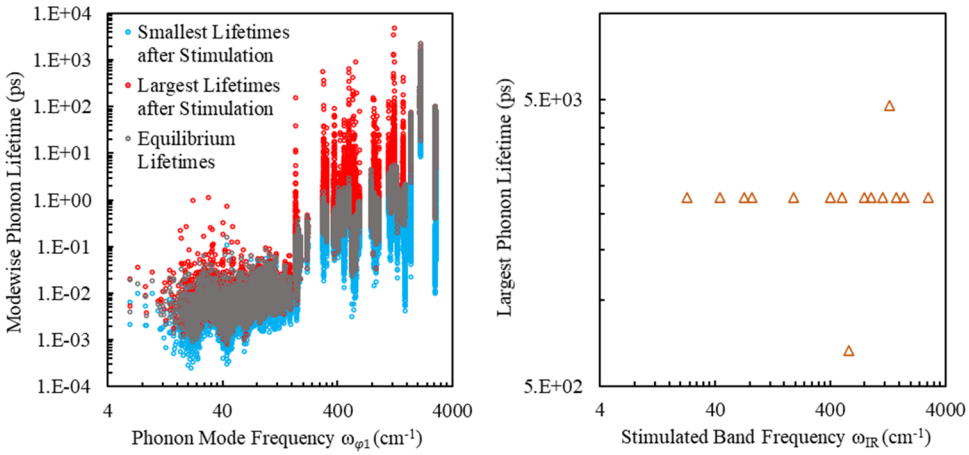

Figure 6. (left) Largest and smallest modewise lifetime values ($\tau^{\Phi_s}_{\phi_\nu,\max}$ and $\tau^{\Phi_s}_{\phi_\nu,\min}$) after stimulating the 15 frequency bands; stimulating the modes can lead to an increase in modewise lifetime values up to four orders of magnitude. The largest % increase in lifetime is observed for several modes around ∼301, from ∼550 to ∼580, ∼838, and 920 cm^{-1}. (Right) Largest phonon lifetime across all 32,256 modes ($\tau^{\Phi_s}_{\phi,\max}$) in RDX upon stimulating each frequency band. The largest phonon lifetime across all 32,256 modes is observed to be 663.88 ps after stimulating the band at 582.36 cm^{-1}, 4784.26 ps after stimulating the band at 1299.72 cm^{-1}, and 2272.90 ps after stimulating all other bands.

as propagating carriers while neglecting the diffusive nature of transport. However, we presently observe that the contribution of each mode to thermal conductivity is proportionally similar in both PGM (propagating carriers) and Allen−Feldman model[71] (diffusive carriers), as shown in Section S4 of the Supporting Information. This implies that proportional changes to mode occupancies through stimulation will affect the scattering behavior, which the present model determines accurately only in a proportional sense. Thus, the relative change in the overall thermal transport is presently accurate even if the precise value of the thermal conductivity is not.

Although the lack of experimental studies investigating the effects of IR radiation on the intrinsic phonon scattering and lattice thermal conductivity in crystalline RDX limits a quantitative comparison of our observations with other published literature. However, qualitatively, our results are consistent with the observations in the existing literature on three levels: (a) The use of ultrafast optical pulses has been shown to control molecular motion and drive the phonon population out of equilibrium in a wide range of materials.[8,24,27,28,47,72−77] Weiner et al. stimulated the low-frequency phonons at 33, 56, 80, and 104 cm^{-1} in the α-perylene molecular crystal using femtosecond pulses. Chapman et al. achieved direct electromagnetic stimulation of transverse-optical phonons at ∼1075 cm^{-1} in quartz via irradiation with a CO_2 laser and observed enhancement of X-ray diffuse scattering due to anharmonic decay from zone-center and zone-boundary phonons.[78] (b) The highly nonequilibrium distribution of phonons has been shown to affect the phonon scattering and vibrational energy-transfer rates.[44,79−83] Following the IR pumping of the T_{1u} mode in a liquid solution of tungsten hexacarbonyl in carbon tetrachloride at 1980 cm^{-1}, Tokmakoff et al. observed phonon scattering rates two orders of magnitude higher than the vibrational energy flow out of the CO stretching modes.[84] Groeneveld et al. investigated the strength of electron−phonon coupling in gold and silver thin films and showed an increase in electron−phonon relaxation time with an increase in laser energy density.[85] (c) Lattice distortion and change in phonon scattering rates due to irradiation have been shown to modify the thermal transport.[25,32,86−90] Alibay et al. demonstrated ignition modulation via microwave stimulation of nAl/MnO_x energetic composites.[91] Senor et al. reported up to 50% reduction and up to 36% increase in the thermal conductivity of various SiC composites upon irradiation due to phonon−phonon and phonon−defect scattering.[92] Chiloyan et al. studied non-diffusive thermal transport at small distances within the Boltzmann transport equation (BTE) framework in single-crystal silicon and reported that nonthermal phonon populations produced by a micro/nanoscale heat source can lead to enhanced heat conductivity.[32] Enhanced thermal conductivity is also observed in the solution of BTE for the pump−probe geometry when interfacial phonon transmission led to nonequilibrium phonon distribution in the silicon substrate.[33] Zhao et al. reported an ∼70% reduction in the thermal conductivity of individual Si nanowires via selective helium ion irradiation due to intrinsic phonon−phonon, phonon−boundary, and phonon−defect scattering.[93] Aring et al. reported a reduction in the thermal conductivity of UO_2 by two orders of magnitude after far-infrared absorption at 17.6, 19.2, 23, 79, and 100 cm^{-1} due to a strong phonon−magnon scattering.[94] Alaie et al. demonstrated a decrease in the thermal conductivity in Si with an increase in the Ga+ ion irradiation dose (up to 10^{16} Ga+/cm^2) due to lattice distortion that modifies the phonon dispersion and scattering rates.[95]

The current work is based on several assumptions such as only the first anharmonic term of the Hamiltonian is considered (three phonon scattering), SMRTA, and the contribution of propagating thermal carriers only is considered (phonon gas model). And therefore, an improvement in the accuracy of the results is expected upon including the contribution of the diffusive carriers, fully nonequilibrium relaxation of phonons, and considering the higher-order phonon scattering events.

CONCLUSIONS

In conclusion, we have shown a proof of concept that based on a highly resolved momentum-dependent calculation of the complete Brillouin zone of a material, selective stimulation of certain low- and mid-frequency phonons can have a substantial positive/negative effect on the thermal diffusivity and conductivity. As phonons are driven out of equilibrium, a

https://doi.org/10.1021/acsomega.1c07364
ACS Omega 2022, 7, 12787−12794

large increase/decrease in the three phonon scattering rates is observed leading to large changes in the phonon mean free paths. Specifically shown in RDX, stimulating the low-frequency band at 22.74 cm^{-1} can lead to a reduction in the thermal conductivity by 12.46%, which may result in increased sensitivity. In contrast, stimulating the mid-frequency bands at 582.36, 1140.67, or 1299.72 cm^{-1} can lead to an increase in the thermal conductivity by 108.45, 144.07, and 23.59%, respectively, which may lead to reduced sensitivity.

COMPUTATIONAL DETAILS

A quantum chemistry-based force field[96] is used to calculate the anharmonic force constants and the harmonic phonon properties over a uniform 6 × 6 × 6 grid of *k*-points under ambient conditions.[61] The details on the convergence of harmonic and anharmonic phonon properties with respect to the number of Brillouin zone sampling points can be found in the Supporting Information of our earlier work.[61] Based on the IR spectroscopy data in the literature,[97−104] 15 IR active modes in RDX spanning the complete phonon spectrum are identified and shown in Table S1. For each IR active mode, a band of discrete modes is defined using the spectral profile shown in Figure S1. The discrete modes that fall within a 1 cm^{-1} linewidth of the listed IR active mode are included in each band. The number of modes included in the band will depend on the choice of the density of *k*-points. Presently, based on the *k*-points selected, a typical band contains roughly 50−60 discrete modes. The index Φ_s is used to represent the bands hereafter.

With recent advances in laser sources, laser fluence on the order of a few eV/A^2 is achievable;[105−108] therefore, an optical energy input (E_{in,Φ_s}) of 1 eV is used for stimulating the phonons in the first band (ω_{IR} = 22.74 cm^{-1}), and since the optical energy of the lasers is proportional to the radiation frequency ($E_{IR} = \hbar\omega_{IR}$), E_{in,Φ_s} is increased linearly with ω_{IR},[12,13,108,109] as shown in Table S2 of the Supporting Information. In addition, the stimulation energy (E_{in,Φ_s}) and % $Absorption_{\Phi_s}$ (Table S1) are assumed constant for all phonon modes within a band. The optical energy absorbed by the phonons in the band Φ_s is calculated as $E_{abs,\Phi_s} = E_{in,\Phi_s} \times$ % $Absorption_{\Phi_s}$, where modewise $\%Absorption_{\Phi_s}$ are obtained from the literature as discussed in section S1 of the Supporting Information. The resulting increase in the population of the phonons due to stimulation is calculated as $\Delta n_{\Phi_s} = E_{abs,\Phi_s}/E_{IR}$, where $E_{IR} = \hbar\omega_{IR}$ and ω_{IR} represent the frequency of the IR active phonon mode.

The change in the scattering rate of a phonon mode ϕ_1 when phonons in the band Φ_S are stimulated can be calculated as

$$\begin{aligned}\Delta\Gamma_{\phi_1}^{\Phi_S} &= \Gamma_{\phi_1}^{\Phi_S} - \Gamma_{\phi_1} \\ &= \sum_{\phi_2,\phi_3\in\Phi_S} \left\{\left(\frac{L_-}{2} - L_+\right)\left(n_{\phi_3}^{S} - n_{\phi_3}^{0}\right)\right\} \\ &\quad + \sum_{\phi_2\in\Phi_S,\phi_3} \left\{\left(\frac{L_-}{2} + L_+\right)\left(n_{\phi_2}^{S} - n_{\phi_2}^{0}\right)\right\}\end{aligned} \quad (1)$$

where $\Gamma_{\phi_1}^{\Phi_S}$ and Γ_{ϕ_1} represent the scattering rates of mode ϕ_1 when phonons in band Φ_S are stimulated and without any phonon stimulation, respectively, ϕ_1, ϕ_2, ϕ_3 are indices for the three phonons involved in the scattering events, L_- represents the strength of emission scattering ($\phi_1 \rightarrow \phi_2 + \phi_3$) and L_+ represents the strength of absorption scattering ($\phi_1 + \phi_2 \rightarrow \phi_3$), n_ϕ^0 represents the equilibrium phonon population of mode ϕ modeled using the Bose−Einstein distribution, and $n_\phi^S = n_\phi^o + \Delta n_{\Phi_S}$ represents the perturbed population of phonon mode ϕ in the stimulated band Φ_S. The details of the three-phonon scattering rate calculation using Fermi's golden rule (FGR) can be found in section S2 of the Supporting Information. Within an incoherent phonon representation, as is used presently, the energy imparted by a radiation source must necessarily result in a positive change in the population of stimulated modes, and the anharmonic coefficients $L_\pm$ and the difference $(n_\phi^S - n_\phi^0)$ must likewise be positive. This implies that the change in the scattering rate in eq 1 for emission processes (L_- terms) is always positive, whereas absorption processes (L_+ terms) can be either positive or negative. Therefore, overall, a stimulation of phonons can induce both positive and negative changes in the intrinsic scattering rates among modes depending on the value of $\left(\frac{L_-}{2} - L_+\right)$ associated with a given triplet of modes. In addition, eq 1 indicates that the change in the scattering rate $\Delta\Gamma_{\phi_1}^{\Phi_S}$ is linearly proportional to the change in phonon population $\Delta n_{\Phi_s} = (n_\phi^S - n_\phi^0)$ and therefore is linearly proportional to the optical energy input E_{in,Φ_s}. Namely, the magnitude of a frustration or stimulation effect will depend on the choice of the optical energy source. It should be noted that stimulation can yield either a positive or negative change in the scattering rate of a given mode. Since the carrier properties are dependent on the chemical interactions and the structural morphology of the material, no simple method appears to exist that can be used to predict whether stimulation of a band will frustrate or stimulate the scattering of any mode.

ASSOCIATED CONTENT

Supporting Information

The Supporting Information is available free of charge at https://pubs.acs.org/doi/10.1021/acsomega.1c07364.

IR active phonon modes in RDX, theoretical and computational details for FGR-based three-phonon scattering, definitions of measures for quantifying the effects of phonon band stimulation, and modewise percent contribution to the thermal conductivity via PGM and Allen−Feldman model (PDF)

AUTHOR INFORMATION

Corresponding Author

Peter W. Chung − *Center for Engineering Concepts Development, Department of Mechanical Engineering, University of Maryland, College Park, Maryland 20742, United States;* orcid.org/0000-0002-3276-5994; Email: pchung15@umd.edu

Author

Gaurav Kumar − *Center for Engineering Concepts Development, Department of Mechanical Engineering, University of Maryland, College Park, Maryland 20742, United States;* Present Address: Purdue University, West Lafayette, Indiana 47907, United States; orcid.org/0000-0002-0935-6383

Complete contact information is available at:

https://doi.org/10.1021/acsomega.1c07364
ACS Omega 2022, 7, 12787−12794

https://pubs.acs.org/10.1021/acsomega.1c07364

Author Contributions

G.K. and P.W.C. conceived the project, G.K. performed the mode stimulation calculations, and G.K. and P.W.C. analyzed the results and wrote the paper. All authors reviewed and have given approval to the final version of the manuscript.

Notes

The authors declare no competing financial interest.

■ ACKNOWLEDGMENTS

G.K. gratefully acknowledges the graduate fellowship from the Center for Engineering Concepts Development and the Kulkarni Foundation Summer Research Fellowship. This work was also supported, in part, by the Department of Mechanical Engineering at the University of Maryland College Park.

■ REFERENCES

(1) Först, M.; Tobey, R. I.; Bromberger, H.; Wilkins, S. B.; Khanna, V.; Caviglia, A. D.; Chuang, Y.-D.; Lee, W. S.; Schlotter, W. F.; Turner, J. J.; Minitti, M. P.; Krupin, O.; Xu, Z. J.; Wen, J. S.; Gu, G. D.; Dhesi, S. S.; Cavalleri, A.; Hill, J. P. Melting of Charge Stripes in Vibrationally Driven La1.875Ba0.125: Assessing the Respective Roles of Electronic and Lattice Order in Frustrated Superconductors. *Phys. Rev. Lett.* **2014**, *112*, No. 157002.

(2) Hu, W.; Kaiser, S.; Nicoletti, D.; Hunt, C. R.; Gierz, I.; Hoffmann, M. C.; le Tacon, M.; Loew, T.; Keimer, B.; Cavalleri, A. Optically Enhanced Coherent Transport in YBa2 Cu3 O 6.5 by Ultrafast Redistribution of Interlayer Coupling. *Nat. Mater.* **2014**, *13*, 705−711.

(3) Fausti, D.; Tobey, R. I.; Dean, N.; Kaiser, S.; Dienst, A.; Hoffmann, M. C.; Pyon, S.; Takayama, T.; Takagi, H.; Cavalleri, A. Light-Induced Superconductivity in a Stripe-Ordered Cuprate. *Science* **2011**, *331*, 189−191.

(4) Mankowsky, R.; Subedi, A.; Först, M.; Mariager, S. O.; Chollet, M.; Lemke, H. T.; Robinson, J. S.; Glownia, J. M.; Minitti, M. P.; Frano, A.; Fechner, M.; Spaldin, N. A.; Loew, T.; Keimer, B.; Georges, A.; Cavalleri, A. Nonlinear Lattice Dynamics as a Basis for Enhanced Superconductivity in YBa2Cu3O6.5. *Nature* **2014**, *516*, 71−73.

(5) Kaiser, S.; Hunt, C. R.; Nicoletti, D.; Hu, W.; Gierz, I.; Liu, H. Y.; le Tacon, M.; Loew, T.; Haug, D.; Keimer, B.; Cavalleri, A. Optically Induced Coherent Transport Far above Tc in Underdoped YBa2Cu3 O6+Î. *Phys. Rev. B* **2014**, *89*, No. 184516.

(6) Rini, M.; Tobey, R.; Dean, N.; Itatani, J.; Tomioka, Y.; Tokura, Y.; Schoenlein, R. W.; Cavalleri, A. Control of the Electronic Phase of a Manganite by Mode-Selective Vibrational Excitation. *Nature* **2007**, *449*, 72−74.

(7) Först, M.; Mankowsky, R.; Cavalleri, A. Mode-Selective Control of the Crystal Lattice. *Acc. Chem. Res.* **2015**, *48*, 380−387.

(8) Mankowsky, R.; Först, M.; Loew, T.; Porras, J.; Keimer, B.; Cavalleri, A. Coherent Modulation of the YB A2 C U3 O6+x Atomic Structure by Displacive Stimulated Ionic Raman Scattering. *Phys. Rev. B* **2015**, *91*, No. 094308.

(9) Först, M.; Manzoni, C.; Kaiser, S.; Tomioka, Y.; Tokura, Y.; Merlin, R.; Cavalleri, A. Nonlinear Phononics as an Ultrafast Route to Lattice Control. *Nat. Phys.* **2011**, *7*, 854−856.

(10) Tobey, R. I.; Prabhakaran, D.; Boothroyd, A. T.; Cavalleri, A. Ultrafast Electronic Phase Transition in La1/2Sr 3/2MnO4 by Coherent Vibrational Excitation: Evidence for Nonthermal Melting of Orbital Order. *Phys. Rev. Lett.* **2008**, *101*, No. 197404.

(11) Okimoto, Y.; Katsufuji, T.; Ishikawa, T.; Arima, T.; Tokura, Y. Variation of Electronic Structure f(0 ⩽ x ⩽ 0.3) as Investigated by Optical Conductivity Spectra. *Phys. Rev. B* **1997**, *55*, 4206−4214.

(12) Grill, W.; Weis, O. Excitation of Coherent and Incoherent Terahertz Phonon Pulses in Quartz Using Infrared Laser Radiation. *Phys. Rev. Lett.* **1975**, *35*, 588−591.

(13) Bron, W. E.; Grill, W. Stimulated Phonon Emission. *Phys. Rev. Lett.* **1978**, *40*, 1459−1463.

(14) Bron, W. E.; Grill, W. Phonon Spectroscopy. II. Spectral, Spatial, and Temporal Evolution of a Phonon Pulse. *Phys. Rev. B* **1977**, *16*, 5315−5320.

(15) Wang, Y.; Ruan, X.; Roy, A. K. Two-Temperature Non-equilibrium Molecular Dynamics Simulation of Thermal Transport across Metal-Nonmetal Interfaces. *Phys. Rev. B* **2012**, *85*, No. 205311.

(16) Dang, N. C.; Gottfried, J. L.; de Lucia, F. C. Energetic Material Response to Ultrafast Indirect Laser Heating. *Appl. Opt.* **2017**, *56*, B85.

(17) Powell, M. S.; Sakano, M. N.; Cawkwell, M. J.; Bowlan, P. R.; Brown, K. E.; Bolme, C. A.; Moore, D. S.; Son, S. F.; Strachan, A.; McGrane, S. D. Insight into the Chemistry of PETN Under Shock Compression Through Ultrafast Broadband Mid-Infrared Absorption Spectroscopy. *J. Phys. Chem. A* **2020**, *124*, 7031−7046.

(18) Dresselhaus-Cooper, L. E.; Martynowych, D. J.; Zhang, F.; Tsay, C.; Ilavsky, J.; Wang, S. G.; Chen, Y.-S.; Nelson, K. A. Pressure-Thresholded Response in Cylindrically Shocked Cyclotrimethylene Trinitramine (RDX). *J. Phys. Chem. A* **2020**, *124*, 3301−3313.

(19) Cole-Filipiak, N. C.; Knepper, R.; Wood, M.; Ramasesha, K. Sub-Picosecond to Sub-Nanosecond Vibrational Energy Transfer Dynamics in Pentaerythritol Tetranitrate. *J. Phys. Chem. Lett.* **2020**, *11*, 6664−6669.

(20) Cole-Filipiak, N. C.; Marquez, M.; Knepper, R.; Harmon, R.; Wiese-Smith, D.; Schrader, P.; Wood, M.; Ramasesha, K. Ultrafast Spectroscopic Studies of Vibrational Energy Transfer in Energetic Materials. *AIP Conf. Proc.* **2020**, *2272*, No. 060006.

(21) Katturi, N. K.; Dev, G. S.; Kommu, N.; Podagatlapalli, G. K.; Soma, V. R. Ultrafast Coherent Anti-Stokes Raman Spectroscopic Studies of Nitro/Nitrogen Rich Aryl-Tetrazole Derivatives. *Chem. Phys. Lett.* **2020**, *756*, No. 137843.

(22) Shi, L.; Yu, P.; Zhao, J.; Wang, J. Ultrafast Intermolecular Vibrational Energy Transfer in Hexahydro-1,3,5-Trinitro-1,3,5-Triazine in Molecular Crystal by 2D IR Spectroscopy. *J. Phys. Chem. C* **2020**, *124*, 2388−2398.

(23) Borrelli, A. Bose—Einstein Statistics. In *Compendium of Quantum Physics*; Springer: Berlin, 2009; Vol. *12*, pp 74−78.

(24) Lu, Z.; Ruan, X. Non-Equilibrium Thermal Transport: A Review of Applications and Simulation Approaches. *ES Energy Environ.* **2019**, *4*, 5−14.

(25) Wang, Y.; Park, J. Y.; Koh, Y. K.; Cahill, D. G. Thermoreflectance of Metal Transducers for Time-Domain Thermoreflectance. *J. Appl. Phys.* **2010**, *108*, No. 043507.

(26) Wilson, R. B.; Cahill, D. G. Anisotropic Failure of Fourier Theory in Time-Domain Thermoreflectance Experiments. *Nat. Commun.* **2014**, *5*, No. 5075.

(27) Johnson, J. A.; Eliason, J. K.; Maznev, A. A.; Luo, T.; Nelson, K. A. Non-Diffusive Thermal Transport in GaAs at Micron Length Scales. *J. Appl. Phys.* **2015**, *118*, No. 155104.

(28) Johnson, J. A.; Maznev, A. A.; Cuffe, J.; Eliason, J. K.; Minnich, A. J.; Kehoe, T.; Torres, C. M. S.; Chen, G.; Nelson, K. A. Direct Measurement of Room-Temperature Nondiffusive Thermal Transport Over Micron Distances in a Silicon Membrane. *Phys. Rev. Lett.* **2013**, *110*, No. 025901.

(29) Pötz, W.; Kocevar, P. Electronic Power Transfer in Pulsed Laser Excitation of Polar Semiconductors. *Phys. Rev. B* **1983**, *28*, 7040−7047.

(30) Ryan, J. F.; Taylor, R. A.; Turberfield, A. J.; Maciel, A.; Worlock, J. M.; Gossard, A. C.; Wiegmann, W. Time-Resolved Photoluminescence of Two-Dimensional Hot Carriers in GaAs-AlGaAs Heterostructures. *Phys. Rev. Lett.* **1984**, *53*, 1841−1844.

(31) Ren, W.; Ouyang, Y.; Jiang, P.; Yu, C.; He, J.; Chen, J. The Impact of Interlayer Rotation on Thermal Transport Across Graphene/Hexagonal Boron Nitride van Der Waals Heterostructure. *Nano Lett.* **2021**, *21*, 2634−2641.

(32) Chiloyan, V.; Huberman, S.; Maznev, A. A.; Nelson, K. A.; Chen, G. Thermal Transport Exceeding Bulk Heat Conduction Due

to Nonthermal Micro/Nanoscale Phonon Populations. *Appl. Phys. Lett.* **2020**, *116*, No. 163102.
(33) Hua, C.; Lindsay, L.; Chen, X.; Minnich, A. J. Generalized Fourier's Law for Nondiffusive Thermal Transport: Theory and Experiment. *Phys. Rev. B* **2019**, *100*, No. 085203.
(34) Chiloyan, V.; Huberman, S.; Maznev, A. A.; Nelson, K. A.; Chen, G. Nondiffusive Thermal Transport from Micro/Nanoscale Sources Producing Nonthermal Phonon Populations Exceeds Fourier Heat Conduction, arXiv:1710.01468. 2017, 1 15.
(35) Mueller, B. Y.; Rethfeld, B. Relaxation Dynamics in Laser-Excited Metals under Nonequilibrium Conditions. *Phys. Rev. B* **2013**, *87*, No. 035139.
(36) Yiğen, S.; Champagne, A. R. Wiedemann−Franz Relation and Thermal-Transistor Effect in Suspended Graphene. *Nano Lett.* **2014**, *14*, 289−293.
(37) Lee, J.-U.; Yoon, D.; Kim, H.; Lee, S. W.; Cheong, H. Thermal Conductivity of Suspended Pristine Graphene Measured by Raman Spectroscopy. *Phys. Rev. B* **2011**, *83*, No. 081419.
(38) Faugeras, C.; Faugeras, B.; Orlita, M.; Potemski, M.; Nair, R. R.; Geim, A. K. Thermal Conductivity of Graphene in Corbino Membrane Geometry. *ACS Nano* **2010**, *4*, 1889−1892.
(39) Cai, W.; Moore, A. L.; Zhu, Y.; Li, X.; Chen, S.; Shi, L.; Ruoff, R. S. Thermal Transport in Suspended and Supported Monolayer Graphene Grown by Chemical Vapor Deposition. *Nano Lett.* **2010**, *10*, 1645−1651.
(40) Balandin, A. A.; Ghosh, S.; Bao, W.; Calizo, I.; Teweldebrhan, D.; Miao, F.; Lau, C. N. Superior Thermal Conductivity of Single-Layer Graphene. *Nano Lett.* **2008**, *8*, 902−907.
(41) Caruso, F. Nonequilibrium Lattice Dynamics in Monolayer MoS2. *J. Phys. Chem. Lett.* **2021**, *12*, 1734−1740.
(42) Seiler, H.; Zahn, D.; Zacharias, M.; Hildebrandt, P. N.; Vasileiadis, T.; Windsor, Y. W.; Qi, Y.; Carbogno, C.; Draxl, C.; Ernstorfer, R.; Caruso, F. Accessing the Anisotropic Nonthermal Phonon Populations in Black Phosphorus. *Nano Lett.* **2021**, *21*, 6171−6178.
(43) Stern, M. J.; René de Cotret, L. P.; Otto, M. R.; Chatelain, R. P.; Boisvert, J.-P.; Sutton, M.; Siwick, B. J. Mapping Momentum-Dependent Electron-Phonon Coupling and Nonequilibrium Phonon Dynamics with Ultrafast Electron Diffuse Scattering. *Phys. Rev. B* **2018**, *97*, No. 165416.
(44) Waldecker, L.; Bertoni, R.; Ernstorfer, R.; Vorberger, J. Electron-Phonon Coupling and Energy Flow in a Simple Metal beyond the Two-Temperature Approximation. *Phys. Rev. X* **2016**, *6*, No. 021003.
(45) Lu, Z.; Vallabhaneni, A.; Cao, B.; Ruan, X. Phonon Branch-Resolved Electron-Phonon Coupling and the Multitemperature Model. *Phys. Rev. B* **2018**, *98*, No. 134309.
(46) Vallabhaneni, A. K.; Singh, D.; Bao, H.; Murthy, J.; Ruan, X. Reliability of Raman Measurements of Thermal Conductivity of Single-Layer Graphene Due to Selective Electron-Phonon Coupling: A First-Principles Study. *Phys. Rev. B* **2016**, *93*, No. 125432.
(47) Sullivan, S.; Vallabhaneni, A.; Kholmanov, I.; Ruan, X.; Murthy, J.; Shi, L. Optical Generation and Detection of Local Nonequilibrium Phonons in Suspended Graphene. *Nano Lett.* **2017**, *17*, 2049−2056.
(48) Zacharias, M.; Seiler, H.; Caruso, F.; Zahn, D.; Giustino, F.; Kelires, P. C.; Ernstorfer, R. Multiphonon Diffuse Scattering in Solids from First Principles: Application to Layered Crystals and Two-Dimensional Materials. *Phys. Rev. B* **2021**, *104*, No. 205109.
(49) Zacharias, M.; Seiler, H.; Caruso, F.; Zahn, D.; Giustino, F.; Kelires, P. C.; Ernstorfer, R. Efficient First-Principles Methodology for the Calculation of the All-Phonon Inelastic Scattering in Solids. *Phys. Rev. Lett.* **2021**, *127*, No. 207401.
(50) Dirac, P. A. M. The Quantum Theory of the Emission and Absorption of Radiation. In *Special Relativity and Quantum Theory*; Springer: Dordrecht, 1988; pp 157−179.
(51) Fried, L. E.; Ruggiero, A. J. Energy Transfer Rates in Primary, Secondary, and Insensitive Explosives. *J. Phys. Chem. A* **1994**, *98*, 9786−9791.
(52) Dlott, D. D.; Fayer, M. D. Shocked Molecular Solids: Vibrational up Pumping, Defect Hot Spot Formation, and the Onset of Chemistry. *J. Chem. Phys.* **1990**, *92*, 3798−3812.
(53) Sharp, K.; Matschinsky, F. Translation of Ludwig Boltzmann's Paper "On the Relationship between the Second Fundamental Theorem of the Mechanical Theory of Heat and Probability Calculations Regarding the Conditions for Thermal Equilibrium" Sitzungberichte Der Kaiserlichen Akademie d. *Entropy* **2015**, *17*, 1971−2009.
(54) McGaughey, A. J. H.; Kaviany, M. Quantitative Validation of the Boltzmann Transport Equation Phonon Thermal Conductivity Model under the Single-Mode Relaxation Time Approximation. *Phys. Rev. B* **2004**, *69*, No. 094303.
(55) Ziman, J. M. *Electrons and Phonons: The Theory of Transport Phenomena in Solids*; Oxford University Press: Oxford, 2001.
(56) Kittel, C. *Introduction to Solid State Physics*; 8th Edition; Wiley & Sons: New York, 2004.
(57) Srivastava, G. P. *The Physics of Phonons*; CRC Press: New York, 2019.
(58) Peierls, R. E.; Roberts, L. D. Quantum Theory of Solids. *Phys. Today* **1956**, *9*, 29.
(59) Wallace, D. C.; Callen, H. Thermodynamics of Crystals. *Am. J. Phys.* **1972**, *40*, 1718−1719.
(60) Dove, M. T.; Condat, C. A. Introduction to Lattice Dynamics. *Am. J. Phys.* **1994**, *62*, 1051−1052.
(61) Kumar, G.; VanGessel, F. G.; Munday, L. B.; Chung, P. W. 3-Phonon Scattering Pathways for Vibrational Energy Transfer in Crystalline RDX. *J. Phys. Chem. A* **2021**, *125*, 7723−7734.
(62) Hill, J. R.; Chronister, E. L.; Chang, T. C.; Kim, H.; Postlewaite, J. C.; Dlott, D. D. Vibrational Relaxation and Vibrational Cooling in Low Temperature Molecular Crystals. *J. Chem. Phys.* **1988**, *88*, 949−967.
(63) Infante-Castillo, R.; Pacheco-Londoño, L.; Hernández-Rivera, S. P. Vibrational Spectra and Structure of RDX and Its 13C- and 15N-Labeled Derivatives: A Theoretical and Experimental Study. *Spectrochim. Acta, Part A* **2010**, *76*, 137−141.
(64) Glenn, R.; Dantus, M. Single Broadband Phase-Shaped Pulse Stimulated Raman Spectroscopy for Standoff Trace Explosive Detection. *J. Phys. Chem. Lett.* **2016**, *7*, 117−125.
(65) McGrane, S. D.; Barber, J.; Quenneville, J. Anharmonic Vibrational Properties of Explosives from Temperature-Dependent Raman. *J. Phys. Chem. A* **2005**, *109*, 9919−9927.
(66) Aubuchon, C. M.; Rector, K. D.; Holmes, W.; Fayer, M. D. Nitro Group Asymmetric Stretching Mode Lifetimes of Molecules Used in Energetic Materials. *Chem. Phys. Lett.* **1999**, *299*, 84−90.
(67) Ostrander, J. S.; Knepper, R.; Tappan, A. S.; Kay, J. J.; Zanni, M. T.; Farrow, D. A. Energy Transfer between Coherently Delocalized States in Thin Films of the Explosive Pentaerythritol Tetranitrate (PETN) Revealed by Two-Dimensional Infrared Spectroscopy. *J. Phys. Chem. B* **2017**, *121*, 1352−1361.
(68) Ramasesha, K.; Knepper, R.; Wood, M.; Cole-Filipiak, N. C. *Experimental and Theoretical Studies of Ultrafast Vibrational Energy Transfer Dynamics in Energetic Materials*; Sandia National Lab: Livermore, CA, USA, 2020.
(69) Kumar, G.; Vangessel, F. G.; Elton, D. C.; Chung, P. W. Phonon Lifetimes and Thermal Conductivity of the Molecular Crystal α-RDX. *MRS Adv.* **2019**, *4*, 2191−2199.
(70) Kumar, G.; VanGessel, F. G.; Chung, P. W. Bond Strain and Rotation Behaviors of Anharmonic Thermal Carriers in -RDX. *Propellants, Explos., Pyrotech.* **2020**, *45*, 169−176.
(71) Allen, P. B.; Feldman, J. L. Thermal Conductivity of Disordered Harmonic Solids. *Phys. Rev. B* **1993**, *48*, 12581−12588.
(72) Nicoletti, D.; Cavalleri, A. Nonlinear Light−Matter Interaction at Terahertz Frequencies. *Adv. Opt. Photonics* **2016**, *8*, 401.
(73) Pfeifer, T.; Kütt, W.; Kurz, H.; Scholz, R. Generation and Detection of Coherent Optical Phonons in Germanium. *Phys. Rev. Lett.* **1992**, *69*, 3248−3251.
(74) Cheng, T. K.; Vidal, J.; Zeiger, H. J.; Dresselhaus, G.; Dresselhaus, M. S.; Ippen, E. P. Mechanism for Displacive Excitation

https://doi.org/10.1021/acsomega.1c07364
ACS Omega 2022, 7, 12787−12794

of Coherent Phonons in Sb, Bi, Te, and Ti2O3. *Appl. Phys. Lett.* **1991**, *59*, 1923−1925.
(75) Kuznetsov, A. V.; Stanton, C. J. Theory of Coherent Phonon Oscillations in Semiconductors. *Phys. Rev. Lett.* **1994**, *73*, 3243−3246.
(76) Nelson, K. A.; Lutz, D. R.; Fayer, M. D.; Madison, L. Laser-Induced Phonon Spectroscopy. Optical Generation of Ultrasonic Waves and Investigation of Electronic Excited-State Interactions in Solids. *Phys. Rev. B* **1981**, *24*, 3261−3275.
(77) Dekorsy, T.; Cho, G. C.; Kurz, H. Coherent Phonons in Condensed Media. In *Light Scattering in Solids VIII*; Spinger: Berlin, 2006; pp 169−209.
(78) Chapman, L. D.; Hsieh, S. M.; Colella, R. X-Ray Evidence of Direct Generation of Nonequilibrium Phonons in Quartz by Infrared Radiation. *Phys. Rev. B* **1984**, *30*, 1094−1096.
(79) Cahill, D. G.; Braun, Pv.; Chen, G.; Clarke, D. R.; Fan, S.; Goodson, K. E.; Keblinski, P.; King, W. P.; Mahan, G. D.; Majumdar, A.; Maris, H. J.; Phillpot, S. R.; Pop, E.; Shi, L. Nanoscale Thermal Transport. II. 2003−2012. *Appl. Phys. Rev.* **2014**, *1*, No. 011305.
(80) Minnich, A. J. Exploring Electron and Phonon Transport at the Nanoscale for Thermoelectric Energy Conversion. Ph. D. Dissertation, Massachusetts Institute of Technology: Cambridge, MA, 2011.
(81) Zhang, Y.; Weber, W. J. Ion Irradiation and Modification: The Role of Coupled Electronic and Nuclear Energy Dissipation and Subsequent Nonequilibrium Processes in Materials. *Appl. Phys. Rev.* **2020**, *7*, No. 041307.
(82) Zhang, Y.; Zhao, S.; Weber, W. J.; Nordlund, K.; Granberg, F.; Djurabekova, F. Atomic-Level Heterogeneity and Defect Dynamics in Concentrated Solid-Solution Alloys. *Curr. Opin. Solid State Mater. Sci.* **2017**, *21*, 221−237.
(83) Zarkadoula, E.; Samolyuk, G.; Xue, H.; Bei, H.; Weber, W. J. Effects of Two-Temperature Model on Cascade Evolution in Ni and NiFe. *Scr. Mater.* **2016**, *124*, 6−10.
(84) Tokmakoff, A.; Sauter, B.; Kwok, A. S.; Fayer, M. D. Phonon-Induced Scattering between Vibrations and Multiphoton Vibrational up-Pumping in Liquid Solution. *Chem. Phys. Lett.* **1994**, *221*, 412−418.
(85) Groeneveld, R. H. M.; Sprik, R.; Lagendijk, A. Femtosecond Spectroscopy of Electron-Electron and Electron-Phonon Energy Relaxation in Ag and Au. *Phys. Rev. B* **1995**, *51*, 11433−11445.
(86) Chernatynskiy, A.; Phillpot, S. R. Evaluation of Computational Techniques for Solving the Boltzmann Transport Equation for Lattice Thermal Conductivity Calculations. *Phys. Rev. B* **2010**, *82*, No. 134301.
(87) Burchell, T. D. Radiation Effects in Graphite and Carbon-Based Materials. *MRS Bull.* **1997**, *22*, 29−35.
(88) Snead, L. L.; Burchell, T. D. Thermal Conductivity Degradation of Graphites Due to Nuetron Irradiation at Low Temperature. *J. Nucl. Mater.* **1995**, *224*, 222−229.
(89) Gallego, N. C.; Burchell, T. D.; Klett, J. W. Irradiation Effects on Graphite Foam. *Carbon* **2006**, *44*, 618−628.
(90) Scott, E. A.; Hattar, K.; Rost, C. M.; Gaskins, J. T.; Fazli, M.; Ganski, C.; Li, C.; Bai, T.; Wang, Y.; Esfarjani, K.; Goorsky, M.; Hopkins, P. E. Phonon Scattering Effects from Point and Extended Defects on Thermal Conductivity Studied via Ion Irradiation of Crystals with Self-Impurities. *Phys. Rev. Mater.* **2018**, *2*, No. 095001.
(91) Alibay, Z.; Olsen, D.; Biswas, P.; England, C.; Xu, F.; Ghildiyal, P.; Zhou, M.; Zachariah, M. R. Microwave Stimulation of Energetic Al-Based Nanoparticle Composites for Ignition Modulation. *ACS Appl. Nano Mater.* **2022**, *5*, 2460−2469.
(92) Senor, D. J.; Youngblood, G. E.; Moore, C. E.; Trimble, D. J.; Woods, J. J.; Newsome, C. E. Effects of Neutron Irradiation on Thermal Conductivity of SiC-Based Composites and Monolithic Ceramics. *Fusion Technol.* **1996**, *30*, 943−955.
(93) Zhao, Y.; Liu, D.; Chen, J.; Zhu, L.; Belianinov, A.; Ovchinnikova, O. S.; Unocic, R. R.; Burch, M. J.; Kim, S.; Hao, H.; Pickard, D. S.; Li, B.; Thong, J. T. L. Engineering the Thermal Conductivity along an Individual Silicon Nanowire by Selective Helium Ion Irradiation. *Nat. Commun.* **2017**, *8*, No. 15919.
(94) Aring, K.; Sievers, A. J. Thermal Conductivity and Far-Infrared Absorption of UO2. *J. Appl. Phys.* **1967**, *38*, 1496−1498.
(95) Alaie, S.; Baboly, M. G.; Jiang, Y. B.; Rempe, S.; Anjum, D. H.; Chaieb, S.; Donovan, B. F.; Giri, A.; Szwejkowski, C. J.; Gaskins, J. T.; Elahi, M. M. M.; Goettler, D. F.; Braun, J.; Hopkins, P. E.; Leseman, Z. C. Reduction and Increase in Thermal Conductivity of Si Irradiated with Ga+ via Focused Ion Beam. *ACS Appl. Mater. Interfaces* **2018**, *10*, 37679−37684.
(96) Smith, G. D.; Bharadwaj, R. K. Quantum Chemistry Based Force Field for Simulations of HMX. *J. Phys. Chem. B* **1999**, *103*, 3570−3575.
(97) Fan, W. H.; Burnett, A.; Upadhya, P. C.; Cunningham, J.; Linfield, E. H.; Davies, A. G. Far-Infrared Spectroscopic Characterization of Explosives for Security Applications Using Broadband Terahertz Time-Domain Spectroscopy. *Appl. Spectrosc.* **2007**, *61*, 638−643.
(98) Allis, D. G.; Zeitler, J. A.; Taday, P. F.; Korter, T. M. Theoretical Analysis of the Solid-State Terahertz Spectrum of the High Explosive RDX. *Chem. Phys. Lett.* **2008**, *463*, 84−89.
(99) Ciezak, J. A.; Jenkins, T. A.; Liu, Z.; Hemley, R. J. High-Pressure Vibrational Spectroscopy of Energetic Materials: Hexahydro-1,3,5-Trinitro-1,3,5-Triazine. *J. Phys. Chem. A* **2007**, *111*, 59−63.
(100) Karpowicz, R. J.; Brill, T. B. Comparison of the Molecular Structure of Hexahydro-1,3,5-Trinitro-s-Triazine in the Vapor, Solution, and Solid Phases. *J. Phys. Chem. A* **1984**, *88*, 348−352.
(101) Karpowicz, R. J.; Sergio, S. T.; Brill, T. B. β-Polymorph of Hexahydro-1,3,5-Trinitro-s-Triazine. a Fourier Transform Infrared Spectroscopy Study of an Energetic Material. *Ind. Eng. Chem. Prod. Res. Dev.* **1983**, *22*, 363−365.
(102) Iqbal, Z.; Suryanarayanan, K.; Suryanarayana, E.; Autera, J. R. *Infrared and Raman Spectra of 1,3,5-Trinitro-1,3,5-Triazacyclohexane (RDX)*; Picatinny Arsenal: Dover, NJ, 1972.
(103) Figueroa-Navedo, A. M.; Ruiz-Caballero, J. L.; Pacheco-Londoño, L. C.; Hernández-Rivera, S. P. Characterization of α- And β-RDX Polymorphs in Crystalline Deposits on Stainless Steel Substrates. *Cryst. Growth Des.* **2016**, *16*, 3631−3638.
(104) da Costa Mattos, E.; Moreira, E. D.; Diniz, M. F.; Dutra, R. C. L.; da Silva, G.; Iha, K.; Teipel, U. Characterization of Polymer-Coated RDX and HMX Particles. *Propellants, Explos., Pyrotech.* **2008**, *33*, 44−50.
(105) Green, B.; Kovalev, S.; Asgekar, V.; Geloni, G.; Lehnert, U.; Golz, T.; Kuntzsch, M.; Bauer, C.; Hauser, J.; Voigtlaender, J.; Wustmann, B.; Koesterke, I.; Schwarz, M.; Freitag, M.; Arnold, A.; Teichert, J.; Justus, M.; Seidel, W.; Ilgner, C.; Awari, N.; Nicoletti, D.; Kaiser, S.; Laplace, Y.; Rajasekaran, S.; Zhang, L.; Winnerl, S.; Schneider, H.; Schay, G.; Lorincz, I.; Rauscher, A. A.; Radu, I.; Mährlein, S.; Kim, T. H.; Lee, J. S.; Kampfrath, T.; Wall, S.; Heberle, J.; Malnasi-Csizmadia, A.; Steiger, A.; Möller, A. S.; Helm, M.; Schramm, U.; Cowan, T.; Michel, P.; Cavalleri, A.; Fisher, A. S.; Stojanovic, N.; Gensch, M. High-Field High-Repetition-Rate Sources for the Coherent THz Control of Matter. *Sci. Rep.* **2016**, *6*, No. 22256.
(106) Nicoletti, D.; Cavalleri, A. Nonlinear Light−Matter Interaction at Terahertz Frequencies. *Adv. Opt. Photonics* **2016**, *8*, 401.
(107) Hoffmann, M. C.; Fülöp, J. A. Intense Ultrashort Terahertz Pulses: Generation and Applications. *J. Phys. D: Appl. Phys.* **2011**, *44*, No. 083001.
(108) Zhou, Z.; Wang, Z.; Huang, W.; Cui, Y.; Li, H.; Wang, M.; Xi, X.; Gao, S.; Wang, Y. Towards High-Power Mid-IR Light Source Tunable from 3.8 to 4.5 Mm by HBr-Filled Hollow-Core Silica Fibres. *Light: Sci. Appl.* **2022**, *11*, No. 15.
(109) Godard, A. Infrared (2−12 Mm) Solid-State Laser Sources: A Review. *C. R. Phys.* **2007**, *8*, 1100−1128.

https://doi.org/10.1021/acsomega.1c07364
ACS Omega 2022, 7, 12787−12794